

Many-Body Correlations Are Non-negligible in Both Fragile and Strong Glassformers

Chengjie Luo^{1,*}, Joshua F. Robinson^{2,3}, Ilian Pihlajamaa¹, Vincent E. Debets¹,

C. Patrick Royall^{4,3,5,6} and Liesbeth M. C. Janssen^{1,†}

¹*Soft Matter and Biological Physics, Department of Applied Physics, Eindhoven University of Technology, P.O. Box 513, 5600 MB Eindhoven, Netherlands*


²*Institut für Physik, Johannes Gutenberg-Universität Mainz, Staudingerweg 7-9, 55128 Mainz, Germany*

³*H. H. Wills Physics Laboratory, University of Bristol, Bristol BS8 1TL, United Kingdom*

⁴*Gulliver UMR CNRS 7083, ESPCI Paris, Université PSL, 75005 Paris, France*

⁵*School of Chemistry, Cantock's Close, University of Bristol, Bristol BS8 1TS, United Kingdom*

⁶*Centre for Nanoscience and Quantum Information, University of Bristol, Bristol BS8 1FD, United Kingdom*

 (Received 26 February 2022; revised 29 June 2022; accepted 23 August 2022; published 28 September 2022)

It is widely believed that the emergence of slow glassy dynamics is encoded in a material's microstructure. First-principles theory [mode-coupling theory (MCT)] is able to predict the dramatic slowdown of the dynamics from only static two-point correlations as input, yet it cannot capture all of the observed dynamical behavior. Here we go beyond two-point spatial correlation functions by extending MCT systematically to include higher-order static and dynamic correlations. We demonstrate that only adding the static triplet direct correlations already qualitatively changes the predicted glass-transition diagram of binary hard spheres and silica. Moreover, we find a nontrivial competition between static triplet correlations that work to *stabilize* the glass state and dynamic higher-order correlations that *destabilize* it for both materials. We conclude that the conventionally neglected static triplet direct correlations as well as higher-order dynamic correlations are, in fact, non-negligible in both fragile and strong glassformers.

DOI: [10.1103/PhysRevLett.129.145501](https://doi.org/10.1103/PhysRevLett.129.145501)

Introduction.—Almost any material can be supercooled or compressed from the liquid to the glass state. During this process, the relaxation dynamics slows down dramatically, while the disordered microstructure undergoes only small changes. This apparent disconnect between structure and dynamics underlies much of the complexity of the glass transition [1–3].

Among the key challenges in tackling the glass transition is the dearth of first-principles theories. Arguably the dominant first-principles theory, mode-coupling theory (MCT) [4–8], does a good job of predicting the increase in structural relaxation time for the first 4–5 decades and indeed can be accurately fitted to experimental [9] and simulation [10] data of *fragile* glassformers in this regime. However, at deeper supercooling, the power-law increase in relaxation time predicted by MCT leads to a total dynamical arrest at state points where experiments and computer simulations still exhibit relaxation [11–13]. Moreover, this power law is completely incompatible with the Arrhenius behavior of *strong* glassformers [14], even at relatively high temperatures. MCT nonetheless predicts qualitatively reliable state diagrams for both fragile and strong glassformers [15,16].

The static structure factor (i.e., two-point density correlations) is normally assumed to be a sufficient representation of the structure to describe a system with pairwise interactions [17], as used in the usual implementation of

MCT. However, it has been shown both experimentally and numerically [12,18–20] that, upon supercooling, higher-order structural motifs change markedly (much more than two-point correlations). Moreover, machine-learning methods identify subtle structural changes [21–24] and configurational entropy drops approaching dynamical arrest [25–27]. Accompanying these subtle changes of structure, it is recognized that higher-order dynamical correlations implicit in so-called cooperatively rearranging regions may enable relaxation at supercoolings past the critical volume fraction ϕ_{MCT} (or critical temperature T_{MCT}) at which MCT predicts the dynamical divergence [3,28]. Given the clear failure of standard MCT to predict dynamical behavior at deep supercooling and these observations of higher-order correlations, there is a clear need to develop a first-principles theory that captures such correlations in a consistent and systematic manner.

The first such attempt to go beyond the two-body level within MCT is to consider static triplet correlations $c^{(3)}$, with $c^{(3)}$ calculated either from simulations [29,30] or theories such as density functional theory [17,31]. In the 1980s, Barrat *et al.* [32] concluded that ϕ_{MCT} for Percus-Yevick hard spheres only quantitatively changes from 0.516 to 0.512 by supplementing MCT with $c^{(3)}$. Later, Sciortino and Kob [30] found that, for both the van Beest-Kramer-van Santen (BKS) model of silica and the Kob-Andersen binary Lennard-Jones model, the inclusion of triplet correlations

improves the prediction of the nonergodicity parameters; the improvement is particularly significant for the former, but at a T_{MCT} that is further removed from the simulated glass-transition temperature. Recently, Ayadim *et al.* [33] discovered that $c^{(3)}$ also quantitatively affects the location of the MCT glass-transition line and the nonergodicity parameter for hard-core particles with short-ranged interactions. These findings hint that many-body correlations such as $c^{(3)}$ could be important for the glassy dynamics of even simple glassformers, but the precise importance and role of such correlations remains ambiguous.

Recently, generalized mode-coupling theory (GMCT) has been developed as a systematic extension of MCT that adds in higher-order dynamic and static correlations [34–38]. Under certain conditions, the hierarchical GMCT framework is even able to account for relaxation behaviors other than the unrealistic power law noted above [39]. So far, within GMCT, only multipoint *dynamic* correlation functions have been incorporated, leading to quantitatively improved critical point predictions with respect to MCT for fragile glassformers. This suggests an improved ability of GMCT to amplify small differences in static structure factors [34–37,40–43]. However, it remains unclear how the combination of *both* structural and dynamic higher-order correlations affects the glassy dynamics from a first-principles perspective.

Here we make a first step toward a full many-body, first-principles treatment of glassy systems by including both static three-body terms and dynamic many-body terms into the GMCT framework. Our method is quite general and can readily be extended to include static four-body and still higher-order terms [44]. We consider two model glassformers from different fragility classes: one is a binary hard sphere mixture (BHS) with a range of size ratios $0.5 \leq \delta \leq 0.8$, and the other is the strong BKS model of silica [45]. We find that $c^{(3)}$ has a non-negligible effect, both quantitatively and qualitatively, on the prediction of the liquid-glass transition even for BHS with small size disparities. Furthermore, the GMCT level of the multipoint *dynamic* correlation functions also qualitatively changes the diagrams of BHS and significantly improves the prediction of relaxation times for SiO_2 , indicating that both static and dynamic multipoint density correlations play a significant and nontrivial role in both glassformers. An implication of our Letter is that the reasonable predictions of MCT for state diagrams and nonergodicity parameters [6], based solely on two-point correlations, could essentially be regarded as a coincidence or a cancellation of errors.

First-principles theory.—We first briefly introduce the GMCT framework. The central dynamic objects for a multicomponent glassy system consisting of \mathcal{N}_p particles and M species are the multicomponent

$2n$ -point density correlation functions $F_{\{\alpha_i\};\{\beta_i\}}^{(2n)}(\{k_i\}, t) = \langle \rho_{-k_1}^{\alpha_1}(0) \rho_{-k_2}^{\alpha_2}(0) \cdots \rho_{-k_n}^{\alpha_n}(0) \rho_{k_1}^{\beta_1}(t) \rho_{k_2}^{\beta_2}(t) \cdots \rho_{k_n}^{\beta_n}(t) \rangle$, where $\rho_k^\alpha(t) = \sum_{i_\alpha=1}^{\mathcal{N}_\alpha} e^{ik \cdot r_{i_\alpha}(t)} / \sqrt{\mathcal{N}_\alpha}$ is a density mode for species $\alpha \in \{1, 2, \dots, M\}$ at wave vector \mathbf{k} and time t , the angular brackets denote an ensemble average, $r_{i_\alpha}(t)$ is the position of particle i_α of species α at time t , and \mathcal{N}_α is the number of particles of type α with $\sum_{\alpha=1}^M \mathcal{N}_\alpha = \mathcal{N}_p$. The label $n \in \{1, 2, \dots, \infty\}$ is the level of the GMCT hierarchy; when $n = 1$, $F_{\alpha\beta}^{(2)}(\mathbf{k}, t)$ is the partial intermediate scattering function. These dynamic equations have been derived from repeated application of the Mori-Zwanzig approach, where we have neglected the off-diagonal correlations [36,37].

The hierarchical equations for $F_{\{\alpha_i\};\{\beta_i\}}^{(2n)}(\{k_i\}, t)$ read [37]

$$\begin{aligned} \ddot{F}_{\{\alpha_i\};\{\beta_i\}}^{(2n)}(t) + F_{\{\alpha_i\};\{\gamma_i\}}^{(2n)}(t) (S_{\{\gamma_i\};\{\theta_i\}}^{(2n)})^{-1} J_{\{\theta_i\};\{\beta_i\}}^{(2n)} \\ + \int_0^t d\tau \dot{F}_{\{\alpha_i\};\{\gamma_i\}}^{(2n)}(t-\tau) (J_{\{\gamma_i\};\{\theta_i\}}^{(2n)})^{-1} K_{\{\theta_i\};\{\beta_i\}}^{(2n)}(\tau) = 0, \end{aligned} \quad (1)$$

where the arguments $\{k_i\}$ and the summation over indices of species are omitted for simplicity. $S_{\{\alpha_i\};\{\beta_i\}}^{(2n)}(\{k_i\}) \equiv F_{\{\alpha_i\};\{\beta_i\}}^{(2n)}(\{k_i\}, t=0)$ is the $2n$ -point static density correlation function describing the microstructure of the system and $J_{\{\alpha_i\};\{\beta_i\}}^{(2n)}(\{k_i\}) = \langle \langle d/dt [\rho_{-k_1}^{\alpha_1} \cdots \rho_{-k_n}^{\alpha_n}] (d/dt) [\rho_{k_1}^{\beta_1} \cdots \rho_{k_n}^{\beta_n}] \rangle \rangle$ is the general static current-current matrix. Both of them contain only even-order density modes, which can be approximated using Gaussian factorization, and hence they only depend on the two-point static density correlations $S_{\alpha\beta}^{(2)}(\mathbf{k})$ [37]. The key unknown part of Eq. (1) is the memory kernel $K^{(2n)}$, which GMCT hierarchically expands as a linear combination of the next-level correlators $F^{(2(n+1))}$ [34,36–38]. That is,

$$\begin{aligned} K_{\{\alpha_i\};\{\beta_i\}}^{(2n)}(\{k_i\}, t) = \frac{\rho}{16\pi^3} \sum_{\mu\nu} \sum_{j=1}^n \int d\mathbf{q} \frac{k_B T}{m_{\alpha_j}} \mathcal{V}_{\mu'\nu'\alpha_j}(\mathbf{q}, \mathbf{k}_j - \mathbf{q}) \\ \times \mathcal{V}_{\mu\nu\beta_j}(\mathbf{q}, \mathbf{k}_j - \mathbf{q}) \frac{k_B T}{m_{\beta_j}} \\ \times F_{\mu'\nu',\{\alpha_i\};\alpha_j,\mu,\nu,\{\beta_i\};\beta_j}^{(2(n+1))}(\mathbf{q}, \mathbf{k}_j - \mathbf{q}, \{k_i\}/k_j, t), \end{aligned} \quad (2)$$

where T is the temperature and m_α is the mass of particle species α . The subscript $\{x_i\}/x_j$ is a list x_1, x_2, \dots, x_n with the specific element x_j removed.

The static vertices, which represent the coupling strength between different wave vectors, are given by [30,37]

$$\begin{aligned} \mathcal{V}_{\alpha\beta\mu}(\mathbf{q}, \mathbf{k} - \mathbf{q}) = \rho k^2 x_\mu c_{\alpha\beta\mu}^{(3)}(\mathbf{q}, \mathbf{k} - \mathbf{q}) \\ + (\mathbf{k} - \mathbf{q}) \cdot \mathbf{k} c_{\beta\mu}^{(2)}(|\mathbf{k} - \mathbf{q}|) \delta_{\alpha\mu} \\ + \mathbf{q} \cdot \mathbf{k} c_{\alpha\mu}^{(2)}(q) \delta_{\beta\mu}, \end{aligned} \quad (3)$$

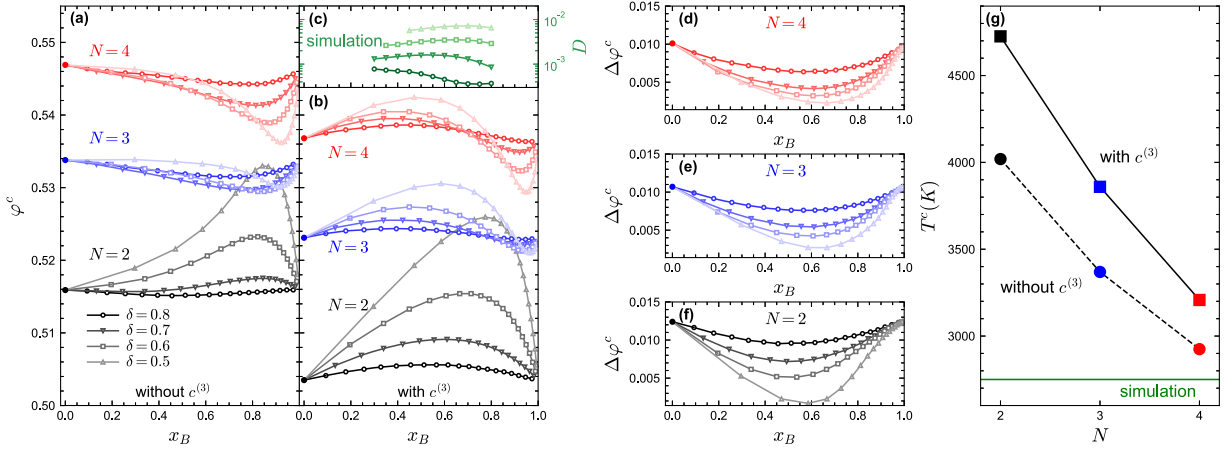


FIG. 1. Liquid-to-glass state diagrams of binary hard spheres as predicted from GMCT (a) without $c^{(3)}$ and (b) with $c^{(3)}$. The curves represent the critical packing fractions φ^c as a function of the number concentration of the small species, $x_B = \mathcal{N}_B/\mathcal{N}_p$. Different symbols correspond to different particle size ratios δ , and different colors correspond to different GMCT closure levels N . (c) The long-time diffusion coefficient D from simulations at packing fraction $\varphi = 0.57$. (d)–(f) The difference of the critical packing fractions without and with $c^{(3)}$, i.e., $\Delta\varphi^c(N, \delta, x_B) = \varphi^c(N, \delta, x_B, \text{without } c^{(3)}) - \varphi^c(N, \delta, x_B, \text{with } c^{(3)})$, as a function of x_B . The filled circles indicate the results for one-component hard spheres. (g) Critical temperature T^c of SiO_2 predicted from GMCT as a function of level N . Squares and circles are with and without $c^{(3)}$, respectively. The solid green line indicates the lowest temperature $T = 2750$ K at which the system can be equilibrated in simulation, and hence it is an upper bound of the glass-transition temperature.

where $x_\mu = \mathcal{N}_\mu/\mathcal{N}_p$ is the number concentration of species μ , $c_{\alpha\beta}^{(2)}(q)$ is the (doublet) direct correlation function connecting to $S^{(2)}$ via the Ornstein-Zernike equation [17,46] and $c_{\alpha\beta\mu}^{(3)}(\mathbf{q}, \mathbf{k} - \mathbf{q})$ is the triplet direct correlation function [30,46].

It is clear now that the inputs to the GMCT framework are only $S^{(2)}$ and $c^{(3)}$, with the latter only appearing in the vertices. To numerically solve the GMCT equations, we follow previous work [36–38] and apply a self-consistent closure for the multipoint dynamic density correlations at the highest level N , such that $F^{(2N)}(t) \approx F^{(2)}(t) \times F^{(2[N-1])}(t)$ (see Supplemental Material [47]). In the following, we report how the inclusion of $c^{(3)}$ and the level N affect the liquid-glass transition for BHS and SiO_2 , as well as the predicted fragility of the latter. As inputs, we take $S^{(2)}$ and $c^{(3)}$ from Rosenfeld’s fundamental measure theory [44,57] for BHS and from molecular dynamics simulations for SiO_2 (see Supplemental Material [47] for details).

Glass-transition diagrams.—We first focus on BHS to discuss the role of the GMCT closure level N . Figures 1(a) and 1(b) show the GMCT-predicted liquid–glass-transition diagrams for several values of the particle size ratio $\delta = d_B/d_A$, where d_A and d_B denote the particle diameters of the larger and smaller species, respectively. Increasing N generally leads to higher critical packing fractions, both with and without $c^{(3)}$, which is consistent with GMCT predictions for monodisperse hard spheres [34,35,40] and sticky hard spheres [42], as well as in better quantitative agreement with the critical points $\varphi^c > 0.58$ reported in experiments and simulations [58–60]. Therefore, regardless

of $c^{(3)}$, including higher-level dynamic density correlations effectively stabilizes the *liquid* state.

Let us check more carefully the effect of N for different size ratios. In standard MCT, i.e., for $N = 2$ and neglecting $c^{(3)}$, two opposite effects are observed at different size disparities [15,61]. Specifically, at a small size disparity such as $\delta = 0.8$ [open circles in Fig. 1(a)], the critical packing fraction is slightly smaller than the monodisperse case (filled circle at $x_B = 0$). However, for a large size disparity such as $\delta = 0.5$ [upward-pointing triangles in Fig. 1(a)], the mixing of the two species leads to higher critical packing fractions. This latter effect is known as entropically induced plasticization and can be attributed to the depletion attraction [59,61]. By increasing N and neglecting $c^{(3)}$, we see that the plasticization effect completely disappears and all curves, in fact, show an inverse-plasticization trend. Contrasting this with the results for small size disparities ($\delta = 0.8$), where the inverse plasticization does not change much as N increases, we can conclude that the effect of N depends on the size ratio and becomes more pronounced for large size disparities.

Interestingly, when we include $c^{(3)}$, the inverse-plasticization effect for $N = 3$ and $N = 4$ without $c^{(3)}$ is inverted again for $x_B \lesssim 0.7$, as can be seen in Fig. 1(b). Notice that, even for MCT ($N = 2$), adding $c^{(3)}$ qualitatively changes the transition curve at small size disparities such as $\delta = 0.8$. Therefore, the triplet direct correlation functions $c^{(3)}$ greatly affect the state diagrams in a non-trivial way.

To delineate the specific effect of $c^{(3)}$ on the glass-transition curves, we plot the difference of the critical

packing fractions without and with $c^{(3)}$, $\Delta\varphi^c = \varphi^c(\text{without } c^{(3)}) - \varphi^c(\text{with } c^{(3)})$, as shown in Figs. 1(d)–1(f). All the differences are positive, which means that, contrary to the role of increasing N , adding $c^{(3)}$ effectively stabilizes the *glass* state. More surprisingly, both the shapes and the magnitudes of the $\Delta\varphi^c$ curves as a function of x_B are similar for all levels N . This may be attributed to the fact that the shapes of the vertices, which contain $c^{(3)}$, remain qualitatively similar for different φ and N (see Supplemental Material [47]). Moreover, for each level N , the largest deviations from the single-component result [$\Delta\varphi^c(x_B = 0)$] are found for the smaller size ratios δ . These results indicate that $c^{(3)}$ plays a larger role with increasing size disparities, similar to the greater effect of level N for large size disparities we discussed before.

To judge whether GMCT gives reasonably good predictions for BHS, we perform event-driven molecular dynamics simulations at high packing fractions [62,63]. Since the shapes of the long-time diffusion coefficient D curves as a function of x_B do not qualitatively change when $\varphi \geq 0.57$ [63], we can regard the diffusion constants at $\varphi = 0.57$ as a semiquantitative indicator for the glass-transition lines, as shown in Fig. 1(c). Qualitatively, MCT without $c^{(3)}$ seems to perform best because both the plasticization effect at small size ratios ($0.5 \leq \delta \leq 0.7$) and the inverse-plasticization effect at large size ratios ($\delta = 0.8$) are observed in the simulations [58], whereas for larger N these two effects are not captured simultaneously. However, if we look more carefully at the location of the peak of D in Fig. 1(c), we can see that, as δ is increased from 0.6 to 0.8, the location of the peak decreases from ~ 0.7 to ~ 0.5 . Without $c^{(3)}$ for $N = 2$ the location of the extremum is not seen to change significantly, whereas incorporating $c^{(3)}$ for $N = 3$ introduces more variation in line with the simulations. Hence, GMCT performs better than MCT at least for certain size ratios. We expect that the good predictions from standard MCT are coincidental, perhaps caused by a fortunate cancellation of errors. We also recall that in the current GMCT framework the multipoint (even-order) static density correlation functions are approximated using Gaussian factorization, the off-diagonal dynamic correlators are ignored [36,37], and the $S^{(2)}$ and $c^{(3)}$ that we use here might be slightly inaccurate compared to simulations [31,44,57]. All of these aspects will affect the accuracy of the state diagrams.

Now let us look at the critical temperature T^c of the strong glassformer SiO_2 predicted from GMCT. From Fig. 1(g) we can see that, both with or without $c^{(3)}$, increasing the level N leads to lower critical temperatures, approaching the glass-transition point. We point out that the T^c at $N = 4$ is even lower than the critical temperature $T_{\text{fit}} = 3330$ K obtained from the power-law fit of diffusion coefficients or α -relaxation times [64,65], unambiguously showing that GMCT is indeed able to go beyond the MCT

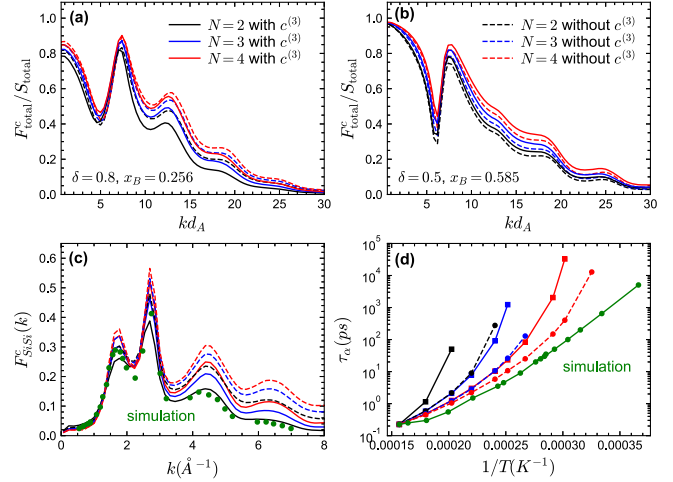


FIG. 2. Critical nonergodicity parameters predicted from GMCT for different closure levels N . The normalized total NEP $F^c_{\text{total}}/S_{\text{total}}$ for BHS where $F^c_{\text{total}} = \sum_{\alpha\beta} F^c_{\alpha\beta}$ and $S_{\text{total}} = \sum_{\alpha\beta} S^{(2)}_{\alpha\beta}$ as a function of the wave number k for (a) $\delta = 0.8$, $x_B = 0.256$ and (b) $\delta = 0.5$, $x_B = 0.585$. In both cases x_B is chosen such that the packing contribution of the small species is $\hat{x}_B = \varphi_B/\varphi = 0.15$. (c) The Si-Si partial NEP $F^c_{\text{SiSi}}(k)$ for SiO_2 at the critical points shown in Fig. 1(g) predicted from GMCT. Green circles are simulation data from [30]. (d) The α -relaxation time τ_α as a function of inverse temperature. τ_α is determined from the partially intermediate scattering function $F_{\text{SiSi}}(k = 1.771 \text{ \AA}^{-1}, \tau_\alpha)/S_{\text{SiSi}}(k = 1.771 \text{ \AA}^{-1}) = e^{-1}$. For better comparison, we scaled the predicted relaxation times for each level N with and without $c^{(3)}$ to make them coincide with the simulated relaxation time at the highest temperature.

regime. However, for a given level N , the critical temperature becomes higher when $c^{(3)}$ is included. Note that the higher temperature of silica corresponds to the lower packing fraction of hard spheres, hence the two competitive effects—that including $c^{(3)}$ stabilizes the glass state, while increasing N stabilizes the liquid state—are universal.

Nonergodicity parameters and fragility.—To further study the roles of the dynamics-related N and the static-related $c^{(3)}$, we consider the nonergodicity parameters (NEPs) at the critical points. Again, we first focus on BHS. In Figs. 2(a) and 2(b), the normalized total NEPs are shown for two different size ratios, $\delta = 0.8$ and $\delta = 0.5$, but at the same packing contribution of the smaller species, i.e., $\hat{x}_B = \varphi_B/\varphi = 0.15$. It can be seen that, for both cases, and both with or without $c^{(3)}$, the NEPs increase as N increases, concurrent with the N -dependent increase in the critical packing fraction.

The effect of $c^{(3)}$ on the NEP is, however, more complex. For $\delta = 0.8$, similar to the monodisperse case (see Fig. S4 [47]), adding $c^{(3)}$ decreases the NEP and hence the relaxation dynamics becomes relatively faster. However, for a small size ratio of $\delta = 0.5$, the opposite effect of $c^{(3)}$ can be observed: when $c^{(3)}$ is included in the vertices, the

NEP increases for a given level N . Note that the critical packing fraction obtained with $c^{(3)}$ is *always* lower than the one without $c^{(3)}$, hence the effect of $c^{(3)}$ on the NEP is not exactly the same as that on the critical packing fractions. In fact, for a large size dispersity of $\delta = 0.5$, the effect of $c^{(3)}$ becomes highly number-concentration dependent (see Fig. S5 [47]). Therefore, consistent with our previous observation that $c^{(3)}$ plays an increasingly important role in the glass-transition diagrams at larger size disparities, we find here that a larger size disparity even produces different effects of $c^{(3)}$ on the NEP. This further confirms that $c^{(3)}$ is non-negligible, especially for large size disparities.

Next we consider the NEP for silica. It is clear from Fig. 2(c) that the effect of $c^{(3)}$ and N on the partial NEP is similar to that on the BHS at a small size disparity $\delta = 0.8$. This is reasonable because the effective size ratio of oxygen and silicon is around 0.84 if we estimate their effective sizes using the first peak position of the corresponding partial radial distribution function [64]. We also note that, for a given level N , adding $c^{(3)}$ always make the NEP closer to the simulation results, which further indicates the important role of $c^{(3)}$.

To illustrate the important role of higher-order dynamic correlations for the glassy dynamics, we finally plot the relaxation times τ_α as a function of inverse temperature, which reflects the fragility of the material, as shown in Fig. 2(d). Contrary to the NEP, the relaxation times predicted from MCT including $c^{(3)}$ deviate most from simulation. The predicted curves substantially come closer to the simulation data when N increases from 2 to 4. Although, in principle, for any finite mean-field closure level N , we can only obtain a power law of the relaxation time near the critical point [41], here we see that GMCT with increasing N is able to improve the shape of the curves over a larger temperature window, i.e., provides a better prediction of the fragility.

Conclusions.—In this Letter, we have made the first step to incorporate both higher-order spatial and temporal correlations into a coherent first-principles framework for the glass transition. Our theory is able to pick up the small structural changes encoded in static multipoint correlation functions to generally improve predictions for the glass transition.

We have demonstrated that static triplet correlations and dynamic multipoint correlations greatly affect the glass transition in a competitive manner for both fragile and strong glassformers. It is well known that static triplet correlations are important for strong glassformers, while high-order dynamic correlations are vital for improving the dynamics of fragile glassformers, but we have shown that the reverse is also true, and hence both static and dynamic many-body correlations are non-negligible in both fragile and strong glassformers. We mention that the many-body correlations in our theory, which are defined in Fourier

space, in principle, contain all information for the corresponding many-body quantities in real space. Hence, one could formally establish a relation with, e.g., locally preferred structures [12,18–20] via a Fourier transform. Our framework should therefore also be sensitive to small structural changes in real space [21–24], but a full real-space analysis is left for future work.

We hypothesize that using additional static higher-order correlations and solving the GMCT equations up to higher closure levels N should bring the predicted glass-transition point and relaxation dynamics closer to the empirical data, but full convergence is currently hampered by the high computational cost associated with such calculations.

We thank Gilles Tarjus for insightful discussions. This work has been financially supported by the Dutch Research Council (NWO) through a START-UP grant (C. L., V. E. D., and L. M. C. J.) and Vidi grant (I. P. and L. M. C. J.). J. F. R. and C. P. R. gratefully acknowledge funding through the European Research Council (ERC consolidator Grant No. NANOPRS, project 617266). C. P. R. acknowledges funding through the ANR grant DiViNew.

*C.Luo@tue.nl

†L.M.C.Janssen@tue.nl

- [1] K. Binder and W. Kob, *Glassy Materials and Disordered Solids: An Introduction to Their Statistical Mechanics* (World Scientific, Singapore, 2011).
- [2] P. G. Debenedetti and F. H. Stillinger, Supercooled liquids and the glass transition, *Nature (London)* **410**, 259 (2001).
- [3] L. Berthier and G. Biroli, Theoretical perspective on the glass transition and amorphous materials, *Rev. Mod. Phys.* **83**, 587 (2011).
- [4] U. Bengtzelius, W. Götze, and A. Sjölander, Dynamics of supercooled liquids and the glass transition, *J. Phys. C* **17**, 5915 (1984).
- [5] E. Leutheusser, Dynamical model of the liquid-glass transition, *Phys. Rev. A* **29**, 2765 (1984).
- [6] W. Götze, *Complex Dynamics of Glass-Forming Liquids: A Mode-Coupling Theory* (Oxford University Press, Oxford, 2009).
- [7] D. R. Reichman and P. Charbonneau, Mode-coupling theory, *J. Stat. Mech.* (2005) P05013.
- [8] L. M. C. Janssen, Mode-coupling theory of the glass transition: A primer, *Front. Phys.* **6**, 97 (2018).
- [9] W. van Meegen, T. C. Mortensen, S. R. Williams, and J. Muller, Measurement of the self-intermediate scattering function of suspensions of hard spherical particles near the glass transition, *Phys. Rev. E* **58**, 6073 (1998).
- [10] W. Kob and H. C. Andersen, Testing mode-coupling theory for a supercooled binary Lennard-Jones mixture. II. Intermediate scattering function and dynamic susceptibility, *Phys. Rev. E* **52**, 4134 (1995).
- [11] G. Brambilla, D. El Masri, M. Pierno, L. Berthier, L. Cipelletti, G. Petekidis, and A. B. Schofield, Probing the

- Equilibrium Dynamics of Colloidal Hard Spheres above the Mode-Coupling Glass Transition, *Phys. Rev. Lett.* **102**, 085703 (2009).
- [12] J. E. Hallett, F. Turci, and C. P. Royall, Local structure in deeply supercooled liquids exhibits growing lengthscales and dynamical correlations, *Nat. Commun.* **9**, 3272 (2018).
- [13] L. Ortlieb, T. S. Ingebrigtsen, J. E. Hallett, F. Turci, and C. P. Royall, Relaxation mechanisms in supercooled liquids past the mode-coupling crossover: Cooperatively re-arranging regions vs excitations, [arXiv:2103.08060](https://arxiv.org/abs/2103.08060).
- [14] C. A. Angell, Structural instability and relaxation in liquid and glassy phases near the fragile liquid limit, *J. Non-Cryst. Solids* **102**, 205 (1988).
- [15] W. Götze and T. Voigtmann, Effect of composition changes on the structural relaxation of a binary mixture, *Phys. Rev. E* **67**, 021502 (2003).
- [16] T. Voigtmann and J. Horbach, The dynamics of silica melts under high pressure: Mode-coupling theory results, *J. Phys. Condens. Matter* **20**, 244117 (2008).
- [17] J.-P. Hansen and I. R. McDonald, *Theory of Simple Liquids* (Elsevier, Amsterdam, 2013).
- [18] M. Leocmach and H. Tanaka, Roles of icosahedral and crystal-like order in the hard spheres glass transition, *Nat. Commun.* **3**, 974 (2012).
- [19] D. Coslovich and G. Pastore, Understanding fragility in supercooled Lennard-Jones mixtures. I. Locally preferred structures, *J. Chem. Phys.* **127**, 124504 (2007).
- [20] Z. Zhang and W. Kob, Revealing the three-dimensional structure of liquids using four-point correlation functions, *Proc. Natl. Acad. Sci. U.S.A.* **117**, 14032 (2020).
- [21] S. S. Schoenholz, E. D. Cubuk, D. M. Sussman, E. Kaxiras, and A. J. Liu, A structural approach to relaxation in glassy liquids, *Nat. Phys.* **12**, 469 (2016).
- [22] V. Bapst, T. Keck, A. Grabska-Barwińska, C. Donner, E. D. Cubuk, S. S. Schoenholz, A. Obika, A. W. Nelson, T. Back, D. Hassabis, and P. Kohli, Unveiling the predictive power of static structure in glassy systems, *Nat. Phys.* **16**, 448 (2020).
- [23] J. Paret, R. L. Jack, and D. Coslovich, Assessing the structural heterogeneity of supercooled liquids through community inference, *J. Chem. Phys.* **152**, 144502 (2020).
- [24] E. Boattini, S. Marín-Aguilar, S. Mitra, G. Foffi, F. Smallenburg, and L. Filion, Autonomously revealing hidden local structures in supercooled liquids, *Nat. Commun.* **11**, 5479 (2020).
- [25] A. Banerjee, S. Sengupta, S. Sastry, and S. M. Bhattacharyya, Role of Structure and Entropy in Determining Differences in Dynamics for Glass Formers with Different Interaction Potentials, *Phys. Rev. Lett.* **113**, 225701 (2014).
- [26] L. Berthier, P. Charbonneau, D. Coslovich, A. Ninarello, M. Ozawa, and S. Yaida, Configurational entropy measurements in extremely supercooled liquids that break the glass ceiling, *Proc. Natl. Acad. Sci. U.S.A.* **114**, 11356 (2017).
- [27] I. Williams, F. Turci, J. E. Hallett, P. Crowther, C. Cammarota, G. Biroli, and C. P. Royall, Experimental determination of configurational entropy in a two-dimensional liquid under random pinning, *J. Phys. Condens. Matter* **30**, 094003 (2018).
- [28] C. P. Royall and S. R. Williams, The role of local structure in dynamical arrest, *Phys. Rep.* **560**, 1 (2015).
- [29] D. Coslovich, Static triplet correlations in glass-forming liquids: A molecular dynamics study, *J. Chem. Phys.* **138**, 12A539 (2013).
- [30] F. Sciortino and W. Kob, Debye-Waller Factor of Liquid Silica: Theory and Simulation, *Phys. Rev. Lett.* **86**, 648 (2001).
- [31] S. Jorge, E. Lomba, and J. Abascal, Theory and simulation of the triplet structure factor and triplet direct correlation functions in binary mixtures, *J. Chem. Phys.* **116**, 730 (2002).
- [32] J. Barrat, W. Gotze, and A. Latz, The liquid-glass transition of the hard-sphere system, *J. Phys. Condens. Matter* **1**, 7163 (1989).
- [33] A. Ayadim, P. Germain, and S. Amokrane, Mode-coupling theory for the glass transition: Test of the convolution approximation for short-range interactions, *Phys. Rev. E* **84**, 061502 (2011).
- [34] G. Szamel, Colloidal Glass Transition: Beyond Mode-Coupling Theory, *Phys. Rev. Lett.* **90**, 228301 (2003).
- [35] J. Wu and J. Cao, High-Order Mode-Coupling Theory for the Colloidal Glass Transition, *Phys. Rev. Lett.* **95**, 078301 (2005).
- [36] L. M. C. Janssen and D. R. Reichman, Microscopic Dynamics of Supercooled Liquids from First Principles, *Phys. Rev. Lett.* **115**, 205701 (2015).
- [37] S. Ciarella, C. Luo, V. E. Debets, and L. M. C. Janssen, Multi-component generalized mode-coupling theory: Predicting dynamics from structure in glassy mixtures, *Eur. Phys. J. E* **44**, 91 (2021).
- [38] V. E. Debets, C. Luo, S. Ciarella, and L. M. C. Janssen, Generalized mode-coupling theory for mixtures of Brownian particles, *Phys. Rev. E* **104**, 065302 (2021).
- [39] P. Mayer, K. Miyazaki, and D. R. Reichman, Cooperativity beyond Caging: Generalized Mode-Coupling Theory, *Phys. Rev. Lett.* **97**, 095702 (2006).
- [40] C. Luo and L. M. C. Janssen, Generalized mode-coupling theory of the glass transition. I. Numerical results for Percus-Yevick hard spheres, *J. Chem. Phys.* **153**, 214507 (2020).
- [41] C. Luo and L. M. C. Janssen, Generalized mode-coupling theory of the glass transition. II. Analytical scaling laws, *J. Chem. Phys.* **153**, 214506 (2020).
- [42] C. Luo and L. M. C. Janssen, Glassy dynamics of sticky hard spheres beyond the mode-coupling regime, *Soft Matter* **17**, 7645 (2021).
- [43] L. Berthier and G. Tarjus, Critical test of the mode-coupling theory of the glass transition, *Phys. Rev. E* **82**, 031502 (2010).
- [44] Y. Rosenfeld, Free-Energy Model for the Inhomogeneous Hard-Sphere Fluid Mixture and Density-Functional Theory of Freezing, *Phys. Rev. Lett.* **63**, 980 (1989).
- [45] B. W. H. van Beest, G. J. Kramer, and R. A. van Santen, Force Fields for Silicas and Aluminophosphates Based on Ab Initio Calculations, *Phys. Rev. Lett.* **64**, 1955 (1990).
- [46] J. Barrat, J. Hansen, and G. Pastore, On the equilibrium structure of dense fluids: Triplet correlations, integral equations and freezing, *Mol. Phys.* **63**, 747 (1988).
- [47] See Supplemental Material at <http://link.aps.org/supplemental/10.1103/PhysRevLett.129.145501> for the

- details on the theories, simulations, and results of this Letter, which includes Refs. [48–56].
- [48] R. A. Biezemans, S. Ciarella, O. Çaylak, B. Baumeier, and L. M. C. Janssen, Glassy dynamics from generalized mode-coupling theory: Existence and uniqueness of solutions for hierarchically coupled integro-differential equations, *J. Stat. Mech.* (2020) 103301.
- [49] L. M. C. Janssen, P. Mayer, and D. R. Reichman, Relaxation patterns in supercooled liquids from generalized mode-coupling theory, *Phys. Rev. E* **90**, 052306 (2014).
- [50] L. M. C. Janssen, P. Mayer, and D. R. Reichman, Generalized mode-coupling theory of the glass transition: Schematic results at finite and infinite order, *J. Stat. Mech.* (2016) 054049.
- [51] E. Flenner and G. Szamel, Relaxation in a glassy binary mixture: Comparison of the mode-coupling theory to a Brownian dynamics simulation, *Phys. Rev. E* **72**, 031508 (2005).
- [52] T. Franosch, M. Fuchs, W. Götze, M. R. Mayr, and A. P. Singh, Asymptotic laws and preasymptotic correction formulas for the relaxation near glass-transition singularities, *Phys. Rev. E* **55**, 7153 (1997).
- [53] J. Lebowitz, Exact solution of generalized Percus-Yevick equation for a mixture of hard spheres, *Phys. Rev.* **133**, A895 (1964).
- [54] G. Foffi, W. Götze, F. Sciortino, P. Tartaglia, and T. Voigtmann, α -relaxation processes in binary hard-sphere mixtures, *Phys. Rev. E* **69**, 011505 (2004).
- [55] T. Voigtmann, Multiple glasses in asymmetric binary hard spheres, *Europhys. Lett.* **96**, 36006 (2011).
- [56] A. P. Thompson, H. M. Aktulga, R. Berger, D. S. Bolintineanu, W. M. Brown, P. S. Crozier, P. J. in't Veld, A. Kohlmeyer, S. G. Moore, T. D. Nguyen *et al.*, LAMMPS—a flexible simulation tool for particle-based materials modeling at the atomic, meso, and continuum scales, *Comput. Phys. Commun.* **271**, 108171 (2022).
- [57] Y. Rosenfeld, D. Levesque, and J.-J. Weis, Free-energy model for the inhomogeneous hard-sphere fluid mixture: Triplet and higher-order direct correlation functions in dense fluids, *J. Chem. Phys.* **92**, 6818 (1990).
- [58] G. Foffi, W. Götze, F. Sciortino, P. Tartaglia, and T. Voigtmann, Mixing Effects for the Structural Relaxation in Binary Hard-Sphere Liquids, *Phys. Rev. Lett.* **91**, 085701 (2003).
- [59] S. R. Williams and W. van Meegen, Motions in binary mixtures of hard colloidal spheres: Melting of the glass, *Phys. Rev. E* **64**, 041502 (2001).
- [60] S. I. Henderson and W. van Meegen, Metastability and Crystallization in Suspensions of Mixtures of Hard Spheres, *Phys. Rev. Lett.* **80**, 877 (1998).
- [61] T. Voigtmann, Mode coupling theory of the glass transition in binary mixtures, Ph.D. thesis, Technische Universität München, 2003.
- [62] M. N. Bannerman, R. Sargant, and L. Lue, Dynamo: A free $\mathcal{O}(n)$ general event-driven molecular dynamics simulator, *J. Comput. Chem.* **32**, 3329 (2011).
- [63] S. Marín-Aguilar, H. H. Wensink, G. Foffi, and F. Smallenburg, Tetrahedrality Dictates Dynamics in Hard Sphere Mixtures, *Phys. Rev. Lett.* **124**, 208005 (2020).
- [64] J. Horbach and W. Kob, Static and dynamic properties of a viscous silica melt, *Phys. Rev. B* **60**, 3169 (1999).
- [65] J. Horbach and W. Kob, Relaxation dynamics of a viscous silica melt: The intermediate scattering functions, *Phys. Rev. E* **64**, 041503 (2001).